A new compressible hyperelastic model for the multi-axial deformation of blood clot occlusions in vessels

Behrooz Fereidoonnezhad[1], Kevin M. Moerman[1], Sarah Johnson[2], Ray McCarthy[2], Patrick J. McGarry[1,]*

[1] Biomedical engineering, National university of Ireland Galway, Galway, Ireland

[2] Cerenovus Galway Neuro-Technology Centre, Johnson & Johnson, Galway, Ireland

Abstract

Mechanical thrombectomy can be significantly affected by the mechanical properties of the occluding thrombus. In this study we provide the first characterization of the volumetric behaviour of blood clots. We propose a new hyperelastic model for the volumetric and isochoric deformation of clot. We demonstrate that the proposed model provides significant improvements over established models in terms of accurate prediction of nonlinear stress-strain and volumetric behaviours of clots with low and high red blood cell compositions. We perform a rigorous investigation of the factors that govern clot occlusion of a tapered vessel. The motivation for such an analysis is two-fold: (i) the role of clot composition on the in-vivo occlusion location is an open clinical question that has significant implications for thrombectomy procedures; (ii) in-vitro measurement of occlusion location in an engineered tapered tube can be used as a quick and simple methodology to assess the mechanical properties/compositions of clots. Simulations demonstrate that both isochoric and volumetric behaviour of clots are key determinants of clot lodgement location, in addition to clot-vessel friction. The proposed formulation is shown to provide accurate predictions of in-vitro measurement of clot occlusion location in a silicone tapered vessel, in addition to accurately predicting the deformed shape of the clot.

Keywords: Acute ischemic stroke, Thrombus, Clot occlusion, Constitutive model, Volumetric behaviour, Thrombectomy

[*] Corresponding author: Patrick.mcgarry@nuigalway.ie

1. Introduction

Acute Ischemic Stroke (AIS), due to embolic occlusion of a cerebral artery, results in over 5.5 million deaths each year. Intra-arterial mechanical thrombectomy (MT) is a minimally invasive procedure in which the obstructing thrombus is removed using a stent-retriever and/or an aspiration catheter. The success of the thrombectomy procedure can be significantly affected by the mechanical properties of the occluding thrombus (Chueh et al. 2011; Johnson et al. 2019). A thrombus or blood clot is made up of a network of fibrin, platelets, red blood cells (RBCs), and other blood components. Clot mechanical properties are strongly influenced by composition and the arrangement of components within the clot. Previous studies have carried out a variety of mechanical testing on thrombus material, including compression testing (Saldívar et al. 2002; Ashton et al. 2009; Krasokha et al. 2010; Chueh et al. 2011; Malone et al. 2018), uniaxial and biaxial tensile testing (Di Martino et al. 1998; Saldívar et al. 2002; Vande Geest et al. 2006; Gasser et al. 2008; Chueh et al. 2011), rheometry (Kim and Srinivasan 2005; van Dam, Evelyne A. Dams, Susanne D. Peters, Gerrit W.M. Rutten, Marcel C.M.; Schurink, Geert Willem H. Buth, Jaap van de Vosse 2006; Malone et al. 2018), nanoindentation (Slaboch et al. 2012; Weafer et al. 2019) and friction testing (Gunning et al. 2018). The extent and composition of the occlusive clot itself influences the therapeutic efficacy of revascularization techniques, yet clot location may also be important because of the nature and degree of collateral compensation beyond the occlusion (Liebeskind 2005).

Computational analysis is widely used for pre-clinical assessment of medical devises (Ajjan et al. 2009; Zhao et al. 2011; Rouhani et al. 2019). In this context, development of accurate biomechanical material models for blood clots is a key for accurate device simulation and analysis. Incompressibility is commonly assumed in computational modelling of soft tissue, though recent investigations have challenged such assumption (Gabbay et al. 2006; McEvoy et al. 2018; Moerman et al. 2020). Blood clots undergo large multi-axial deformations during vessel occlusion, and also during thrombectomy procedures. However, the relative contributions of volumetric and isochoric material behaviour have not previously been investigated.

Therefore, the main motivations/objectives of this study are as follows:

1. Develop and validate a new material model for the volumetric and isochoric mechanical behaviour of blood clots.

2. Investigate the relationship between clot composition/mechanical behaviour and the location at which a clot occlusion occurs in a tapered vessel.

The paper is structured as follows. In Section 2, we calculate the volume change of blood clot analogues during unconfined compression tests for two clot compositions: a fibrin-rich made from a 5% haematocrit (H) blood mixture; and a RBC-rich clot made from a 40% H blood mixture. A new volumetric and isochoric hyperelastic model for clots is presented and is shown to accurately reproduce non-linear stress-strain data and non-linear volumetric data for both compositions. In Section 3 we investigate the influence of clot mechanical properties on occlusion location in a tapered vessel. Following a preliminary analysis to clearly parse the sensitivity of the final lodged position of the clot to isochoric and volumetric deformation regimes, we demonstrate that the new constitutive material model accurately replicates clot occlusion locations measured in vitro. Finally, we simulate clot occlusion in a patient-specific artery.

2. Constitutive modelling of blood clots

2.1. Constitutive law for isochoric and volumetric behaviour of blood clots

The hyperelastic model recently proposed by Fereidoonnezhad and McGarry (2020) is extended to model the volumetric and isochoric behaviour of blood clots. The isochoric strain energy density function is given as

$$\psi_{iso}(\bar{\lambda}_1,\bar{\lambda}_2,\bar{\lambda}_3)=\sum_{i=1}^{3}\bar{\psi}(\bar{\lambda}_i),$$

$$\bar{\psi}(\bar{\lambda}_i)=\begin{cases} E_1\left(\bar{\lambda}_i-\ln\bar{\lambda}_i-1\right) & |\bar{\lambda}_i-1|\le D_1 \\ p\left(\dfrac{\bar{\lambda}_i^{\,2}}{2}-2\bar{\lambda}_i+\ln\bar{\lambda}_i\right)+q\left(\bar{\lambda}_i-\ln\bar{\lambda}_i\right)+r\ln\bar{\lambda}_i+\psi_{01} & D_1<|\bar{\lambda}_i-1|<D_2 \\ E_2\left(\bar{\lambda}_i-(1+D_2)\ln\bar{\lambda}_i\right)+(pD_2^2+qD_2+r)\ln\bar{\lambda}_i+\psi_{02} & |\bar{\lambda}_i-1|\ge D_2 \end{cases} \quad (1)$$

where $D_1, D_2, E_1,$ and E_2 are material parameters, λ_i $(i=1,2,3)$ are the three principal stretches, $\bar{\lambda}_i$ $(i=1,2,3)$ are the isochoric principal stretches, $J=\lambda_1\lambda_2\lambda_3$ is the jacobian, and ψ_{01} and ψ_{02} are two constants which ensure the continuity of strain energy.

Moreover p, q, and r are not independent parameters; in order to maintain C^0 and C^1 continuity the following relations must be enforced:

$$p = \frac{E_1 - E_2}{2(D_1 - D_2)}, \quad q = E_1 - 2D_1 p, \quad r = (E_1 - q)D_1 - pD_1^2 \tag{2}$$

In the current study we propose an extension of this framework to account for non-linear volumetric behaviour. Building upon to equation (1), a new volumetric strain energy density function is implemented such that:

$$\psi_{vol}(J) = \begin{cases} \kappa_1(\mathrm{J} - \ln \mathrm{J} - 1) & |\mathrm{J} - 1| \leq D_{1v} \\ p_v\left(\frac{\mathrm{J}^2}{2} - 2J + \ln \mathrm{J}\right) + q_v(\mathrm{J} - \ln \mathrm{J}) + r_v \ln \mathrm{J} + \psi_{01v} & D_{1v} < |\mathrm{J} - 1| < D_{2v} \\ \kappa_2(\mathrm{J} - (1 + D_{2v}) \ln \mathrm{J}) + (p_v D_{2v}^2 + q_v D_{2v} + r_v) \ln \mathrm{J} + \psi_{02v} & |\mathrm{J} - 1| \geq D_{2v} \end{cases} \tag{3}$$

in which κ_1 and κ_2 are the initial small-strain and large-strain bulk modulus, respectively, the parameters D_{1v} and D_{2v} control the transition volumetric strains, and p_v, q_v, and r_v are obtained in a similar manner as equation (2) by using the corresponding volumetric parameters. The total strain energy density of the clot material is given as $\psi = \psi_{iso}(\bar{\lambda}_1, \bar{\lambda}_2, \bar{\lambda}_3) + \psi_{vol}(J)$. Stress-strain relationships are readily derived from (1) and (2) above, as described by Fereidoonnezhad and McGarry (2020). Sensitivity analysis of the proposed model in terms of the isochoric and volumetric parameters have been performed and the results are presented in Appendix A.

2.2. Experimental characterisation of clots and of constitutive law calibration

In Fig.1 we demonstrate that the proposed material formulation accurately reproduces experimentally observed nominal stress-strain behaviour of blood clots subjected to unconfined compression (Johnson et al. 2020).

Clot analogues have been fabricated from fresh ovine blood which has been found to be a suitable substitute for human blood (Duffy et al. 2017). Citrated whole blood was used to form platelet-contracted blood clots within 5 hours of blood collection from the donor animals. Test samples were then prepared by cutting the clots into cylindrical-shaped samples with an approximate diameter of 10 mm, and an approximate height of 5 mm. Unconfined compression was used to determine the material behaviour of

the analogue clot samples, the day after formation (minimum of n ≥15 for each clot type). The testing was performed on a Zwick uniaxial tensile machine (Zwick Z2.5, Ulm, Germany), using a customised aluminium platen. The samples were placed between two platens and the crosshead position of the machine was adjusted so that the top platen was slightly touching the top of the sample at the beginning of the test. The Specimens are deformed to a nominal compressive axial strain of -0.8 at a compressive strain rate of 0.1 s^{-1} (Fig.1A). The reader is referred to the recent study of Johnson et al. (2020b) for a full description of the fabrication protocols and testing method for clot analogues.

Fig.1C and E show the experimentally measured stress-strain behaviour for a RBC rich and fibrin-rich clot subjected to unconfined compression, respectively. In the current study, using video imaging of the experimental tests of Johnson et al. (2020b), we determine the volume changes of the clot during compression using a customised image analysis programme developed in Matlab (Nolan and McGarry 2016; McEvoy et al. 2018). The height and diameter of the cylindrical clot specimen at different time steps are obtained from the video, and the corresponding compressive axial strain ($\epsilon_a = \lambda_a - 1$) and volumetric strain ($\epsilon_v = J - 1$) are calculated. No previous study reported the volume change of clot and this is the first effort to measure and report the volume change in compression test for blood clots. A highly non-linear relationship between volumetric strain and compressive axial strain is shown in Fig.1D for the RBC rich clot. Initial axial deformation results in a high rate of volume change (w.r.t applied axial strain, $d\epsilon_v/d\epsilon_a$), suggesting an initially low bulk modulus. However, a significantly lower rate of volume change is observed for the applied range of axial strain of $0.1 \leq \epsilon_a \leq 0.48$. Finally, the rate of volume change reaches a higher value for $\epsilon_a \geq 0.48$. Full recovery of volumetric strain is observed following retraction of the loading plate.

We have then simulated the compression test by using the proposed model and fit the $\sigma_a - \epsilon_a$ and $\epsilon_v - \epsilon_a$ curves to the corresponding experimental results, using the nonlinear least-square method in Matlab. Optimised parameters for fibrin-rich clot and RBC-rich clot are provided in Table 1. Model predictions of the clot stress-strain behaviour and volume change are superimposed on Fig.1C-D. The model accurately reproduces the observed complex non-linear experimental behaviour, both in terms of

computed nominal stress σ_a (R^2= 0.997) and ε_v (R^2= 0.978), for the entire range of applied axial deformation. Model results suggest that effective tri-linear relationship between ε_v and ε_a, observed experimentally, emerges due to the interaction of material isochoric stiffening and volumetric stiffening. Similar results are presented for fibrin-rich 5% H clots in Fig.1 E-F, again with evidence of bi-linear strain stiffening (Fig.1E). A corresponding increase in the rate of volume change is observed (Fig.1F), such that $d\epsilon_v/d\epsilon_a = 0.0718$ if $\epsilon_a < 0.35$ and $d\epsilon_v/d\epsilon_a = 0.8141$ if $\epsilon_a > 0.55$. However, as shown in Fig.1F, a bi-linear, rather than tri-linear, relationship between ε_v and ε_a is observed experimentally for fibrin-rich 5% H clots ($d\epsilon_v/d\epsilon_a = 0.0718$ for $\epsilon_a < 0.35$ and $d\epsilon_v/d\epsilon_a = 0.8141$ for $\epsilon_a > 0.55$). Again, the computational model accurately reproduces the complex non-linear clot behaviour over the large range of applied axial strain, both in terms of σ_a (R^2= 0.986) and ϵ_v (R^2= 0.957). Best-fit model parameters are listed in Table 1. The experimental and computational investigation of volumetric behaviour of blood clots presented in Fig.1 provides new insight into a key feature of clot behaviour. Previous studies have been limited to the simplified assumption of near incompressible behaviour.

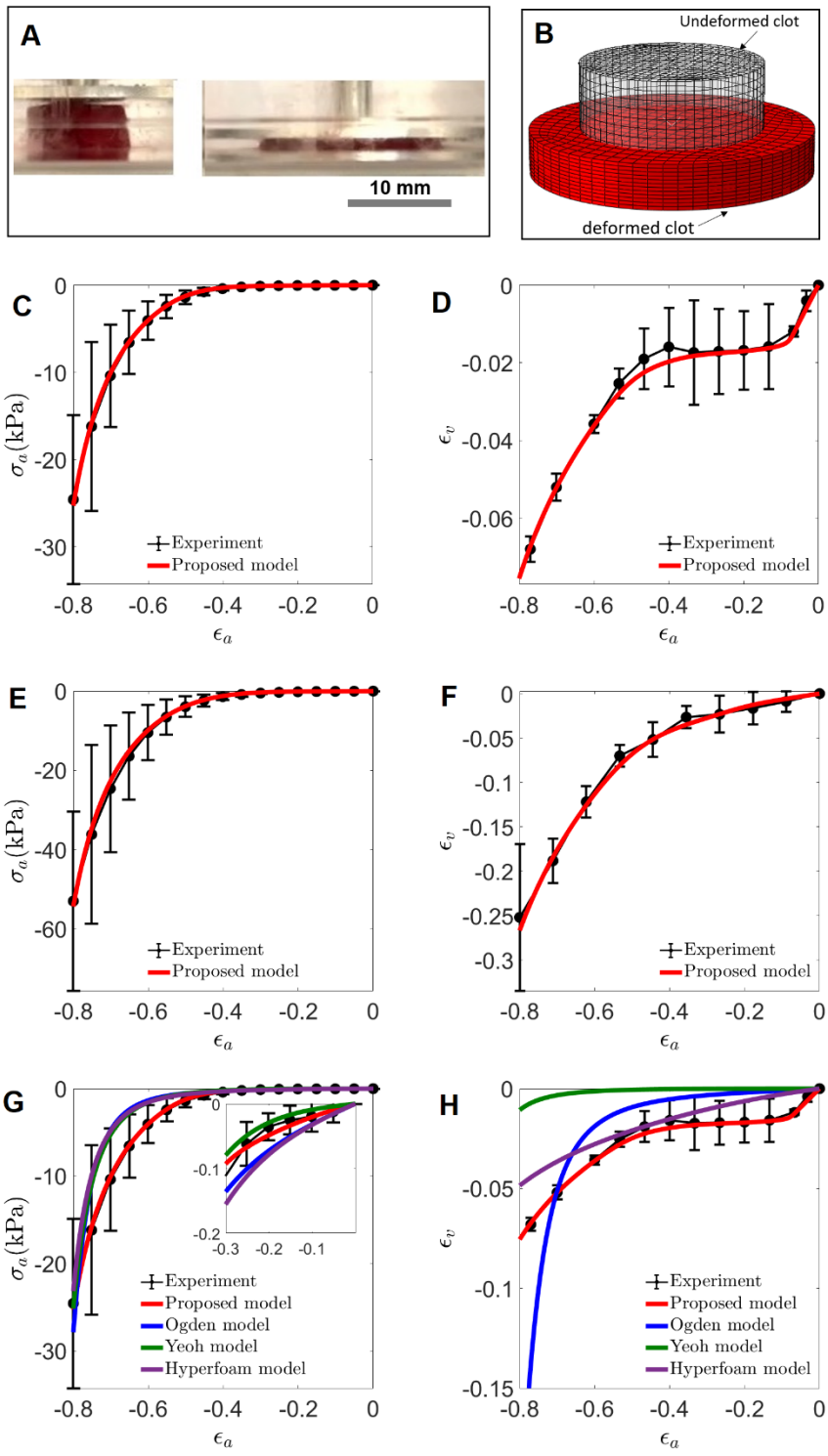

Fig.1*: The capability of the proposed model to reproduce the stress-strain experimental data of the unconfined compression of 5% H and 40%H platelet-contracted blood clot analogues* (Johnson et al. 2020)*. (A) undeformed and deformed blood clot during unconfined compression test; (B) FE simulation of the unconfined compression test; (C, D) Nominal Stress-nominal strain data* (Johnson et al. 2020) *and volume change for a RBC-rich platelet-contracted clot made from 40% H blood*

mixture, (E, F) Nominal Stress-nominal strain data (Johnson et al. 2020) *and volume change for a fibrin-rich platelet-contracted clot made from a 5% H blood mixture. (G, H) Comparing the capability of the proposed model with the well-known hyperelastic laws in reproducing the nominal stress-strain data and the volume change, for the RBC-rich clot analogue.*

***Table 1**: Material parameters of the proposed model for Fibrin-rich and the RBC-rich platelet-contracted clot analogues.*

	D_1	D_2	$E_1\,[kPa]$	$E_2\,[kPa]$	D_{1v}	D_{2v}	$\kappa_1\,[kPa]$	$\kappa_2\,[kPa]$
Fibrin-Rich	0.13	0.59	0.3	9	0.01	0.05	2	15
RBC-Rich	0.25	0.55	0.15	4.1	0.014	0.022	0.5	29

In Fig.1 (G,H) we demonstrate that well established and widely implemented hyperelastic formulations are not capable of accurately predicting the non-linear multi-axial behaviour of blood clots shown in Fig.1 above, in contrast to the accurate and robust predictions of our proposed model. Specifically, the Yeoh, Ogden and hyperfoam formulations are investigated. Fig.1 (G,H) presents the best-fit prediction for each model, subject to the constraint that all models are calibrated to reproduce experimental value of axial stress at the maximum value of applied axial strain ($\epsilon_a = -0.8$), and the initial axial compressive stiffness ($d\sigma_a/d\epsilon_a\,; -0.1 \leq \epsilon_a \leq 0.0$). Established model formulations and best-fit parameters are presented in Appendix B. In contrast to our proposed formulation, Fig.1G shows that all established models inaccurately predict the tangent stiffness and stress throughout the applied range of ϵ_a. Corresponding predictions of volume change are highly inaccurate for all models for all levels of applied axial strain, as shown in Fig.1H. The inaccuracy of each formulation is quantified in Table 2, in terms of predicted axial stress (σ_a), tangent stiffness, and volumetric strain (ϵ_v) at applied axial strains of 20%, 60%, and 80%. The superior accuracy of the proposed model suggests that blood clots transition from a

low constant stiffness regime at low strains to a high constant stiffness regime at high strains, rather than exhibiting continuous power-law or exponential strain stiffening. The accuracy of the non-linear volumetric component of our model suggests that a single parameter (bulk modulus) linear volumetric constitutive law is insufficient for the accurate simulation of large multiaxial large-deformation of clots. In the following sections we demonstrate that both the isochoric and the volumetric behaviour of blood clots are key determinants of the location of clot lodgement in a tapered vessel, thus highlighting the importance of the results presented in Fig.1.

***Table 2**: Comparing model predictions (proposed (prop.), Ogden, Yeoh, Hyperfoam models) with experimental data for unconfined compression tests of RBC-rich platelet-contracted clot analogues. The values of nominal axial stress (σ_a), stiffness, and volumetric strain (ϵ_v) at 20%, 60%, and 80% axial compressive strain (ϵ_a) are given. Model errors (%) with respect to experimental data are also indicated.*

	$\epsilon_a = 20\%$	$\epsilon_a = 60\%$	$\epsilon_a = 80\%$
	$\sigma_a(kPa)$ [% error]		
Experiment	0.04	4.06	24.58
Prop. model	0.05 [25%]	4.03 [0.8%]	25.28 [2.8%]
Ogden	0.07 [75%]	1.78 [56%]	23.75 [-3.4%]
Yeoh	0.03 [-25%]	1.57 [-62%]	25.17 [2.4%]
Hyperfoam	0.07 [75%]	1.45 [-64%]	24.51 [-0.3%]
	Tangent stiffness (kPa) [% error]		
Experiment	0.37	41.51	171.75
Prop. model	0.33 [-10%]	41.28 [-0.5%]	201.82 [18%]
Ogden	0.56 [53%]	18.90 [-55%]	318.77 [86%]
Yeoh	0.31 [-17%]	17.25 [-58%]	434.45 [153%]
Hyperfoam	0.53 [45%]	14.56 [-65%]	459.65 [168%]
	ϵ_v (%) [% error]		
Experiment	1.68	3.58	6.80
Prop. model	1.70 [1%]	3.62 [1%]	6.80 [0%]
Ogden	0.39 [-77%]	4.97 [39%]	30.51 [350%]
Yeoh	0.005 [-100%]	0.13 [-96%]	0.78 [-89%]
Hyperfoam	0.89 [-47%]	3.60 [1%]	5.81 [-15%]

3. Analysis of the lodgement of blood clots in a tapered vessel

In this section we investigate the influence of clot mechanical properties on the occlusion location in a tapered vessel. The motivation for such an analysis are two-fold: (i) the role of clot composition on the in-vivo occlusion location is a key and open clinical question that could potentially have significant implications for thrombectomy procedures; (ii) in-vitro benchtop measurement of occlusion location in an engineered tapered tube can potentially be used as a quick and simple methodology to assess the mechanical properties/compositions of excised clots or fabricated clot analogues. In the preliminary analysis of Section 3.1 we initially restrict our analysis to quasi-linear material behaviour (i.e. approximately constant stiffness), for both isochoric (shape changing) and volumetric deformation in order to clearly parse the sensitivity of the final lodged position of the clot to both deformation regimes. In Section 3.2 we incorporate non-linear material behaviour, using the calibrated novel constitutive law presented in Section 2 above. We also consider the role of clot rate-dependent visco-hyperelastic on the time-scale required for a clot to reach its final lodged position in Appendix C.

The proposed constitutive model has been implemented into the commercial nonlinear Finite Element (FE) software abaqus/standard (2017) via user subroutine UMAT. Axisymmetric FE simulations have been used for all simulations in this paper except for the patient-specific simulation in Section 3.3 where a 3D simulation has been performed. The CAX4 elements have been used for clot and tapered tube assumed as a rigid body. A frictional contact has been considered between clot and tube.

Convergence of the results in terms of the number of elements has been performed and it is found that element size of 0.09 mm is small enough for convergence of the results. The number of elements is different in each simulation depends on the length of the clot. More details of the mesh study is presented in Appendix D.

3.1. Linear isochoric and volumetric mechanical behaviour

In this section we consider a linear behaviour for the clot to investigate the governing parameters in the occlusion location of clot in a tapered vessel and to provide a proof

of concept for the nonlinear interactions between governing parameters. Therefore, the values of parameters in this section are not necessarily in the physiological range.

Method

Fig.2 presents a schematic of the clot and vessel, indicating the key geometric parameters that describe the system and the pressure P_0 applied to the proximal surface of the clot. Several mechanisms govern the final equilibrium position of the clot in the vessel: friction between the clot and the vessel wall, the isochoric deformability of the clot (characterised by the shear modulus $\mu = 3\kappa E/(9\kappa - E)$), and the volumetric compressibility of the clot (characterised by the bulk modulus κ). The equilibrium occlusion location is characterised by the distance u between the centre of the clot at initial contact with the vessel and centre of the clot at its final equilibrium position. It should be noted that we present our computed results in non-dimension quantities in order to efficiently demonstrate the key parameter groupings that govern the final equilibrium position of the clot. As a simple example, consider a large and a small clot, both with the same aspect ratio L/D. Of course both clots will initially contact the vessel at different locations, and the larger clot will move a greater distance u to its final equilibrium position. However, u/D, the non-dimensional measure of the clots' final positions, will obviously be identical in both cases; i.e. for a given clot aspect ratio, u scales with the size of the clot.

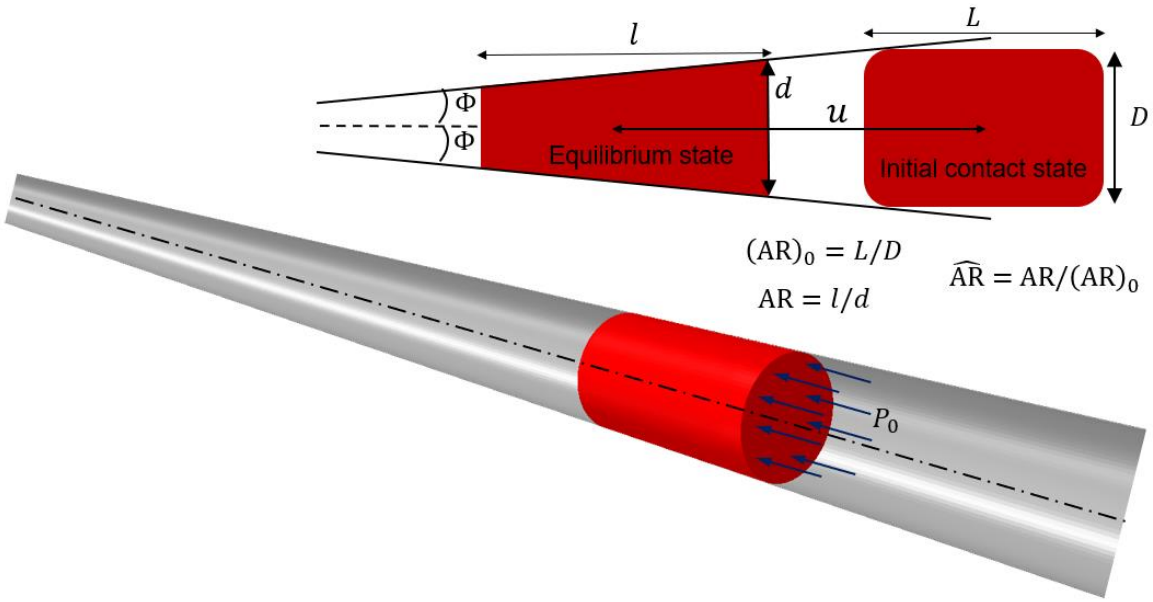

***Fig.2**: A schematic illustration of the occlusion of a cylindrical blood clot in a tapered vessel. Aspect ratio of clot at initial contact state ($(AR)_0$) and at equilibrium state (AR) as well as the normalized aspect ratio ($\widehat{AR}$) are defined.*

Influence of material properties

Fig.3 shows the results of preliminary parametric study for a vessel with the taper angle of $\Phi = 2^o$. As shown in Fig.3A1, the location of clot lodgement, u, (i.e. the equilibrium position of the clot) for a given applied pressure is strongly dependent on the clot shear modulus for nearly incompressible clots because, in this case, clot cannot change volume and the only deformation mechanism is isochoric shape change, governed by the shear modulus. However, for the case of compressible clots, as shown in Fig.3D1, the final lodged position is not strongly influenced by shear modulus; volume change becomes the dominant mode of deformation. In the physiological cerebral artery blood pressure range (60-100 mmHg (Pires et al. 2013)) a five-fold increase in shear modulus from 1kPa to 5kPa results in a ~48% decrease in u if a clot is nearly incompressible (Fig.3A1), compared to a ~14% decrease if the clot is compressible (Fig.3D1). It is noted that the range shear modulus (in the small deformation regime) for excised blood clots extends from 18.6 kPa for platelet contracted/fibrin rich clots down to 0.34 kPa for non-contracted red blood cell rich clots, based on mechanical testing and constitutive modelling of excised clots. The interaction between isochoric and volumetric parameters is further illustrated in Fig.3B1 ($\mu = 5\ kPa$) and Fig.3E1 ($\mu = 50\ kPa$). Beyond a certain level of compressibility ($\kappa \gtrsim 150\ kPa$) the lodged position, u, is insensitive to the value of κ, but strongly dependent on μ (i.e. nearly incompressible clots behave in a similar manner to fully incompressible clots, as demonstrated by the computed value of u for $\kappa = 150\ kPa$ (nearly incompressible) and $\kappa = 2500\ kPa$ (essentially fully incompressible)). However, when the clot is highly compressible, the value of bulk modulus significantly influences the final position; i.e. if kappa is reduced from $150\ kPa$ (nearly incompressible) to $25\ kPa$ (highly compressible), u increases by 45% for low values of shear modulus (Fig.3B) and 62% for high values of shear modulus (Fig.3E1).

Influence of friction coefficient

Fig.3C1, F1 present a preliminary study of the influence of friction coefficient, f, between the clot and the vessel wall for compressible and nearly incompressible clots, respectively. As expected, u increases with decreasing values of f in both cases. However, even for the quasi-linear material behaviour assumed for this preliminary investigation, for any given value of applied pressure P_0, the relationship between f and u is computed to be non-linear. A previous experimental study (Gunning et al. 2018) suggests that the value of f depends on the clot composition; i.e., fibrin-rich blood clots have higher friction coefficient with vessel wall than the RBC-rich clots. More discussion on the friction coefficient is provided in section 3.3. Influence of the shear modulus, bulk modules and friction coefficient on the length of the clots are also provided in Fig.3B2-G2.

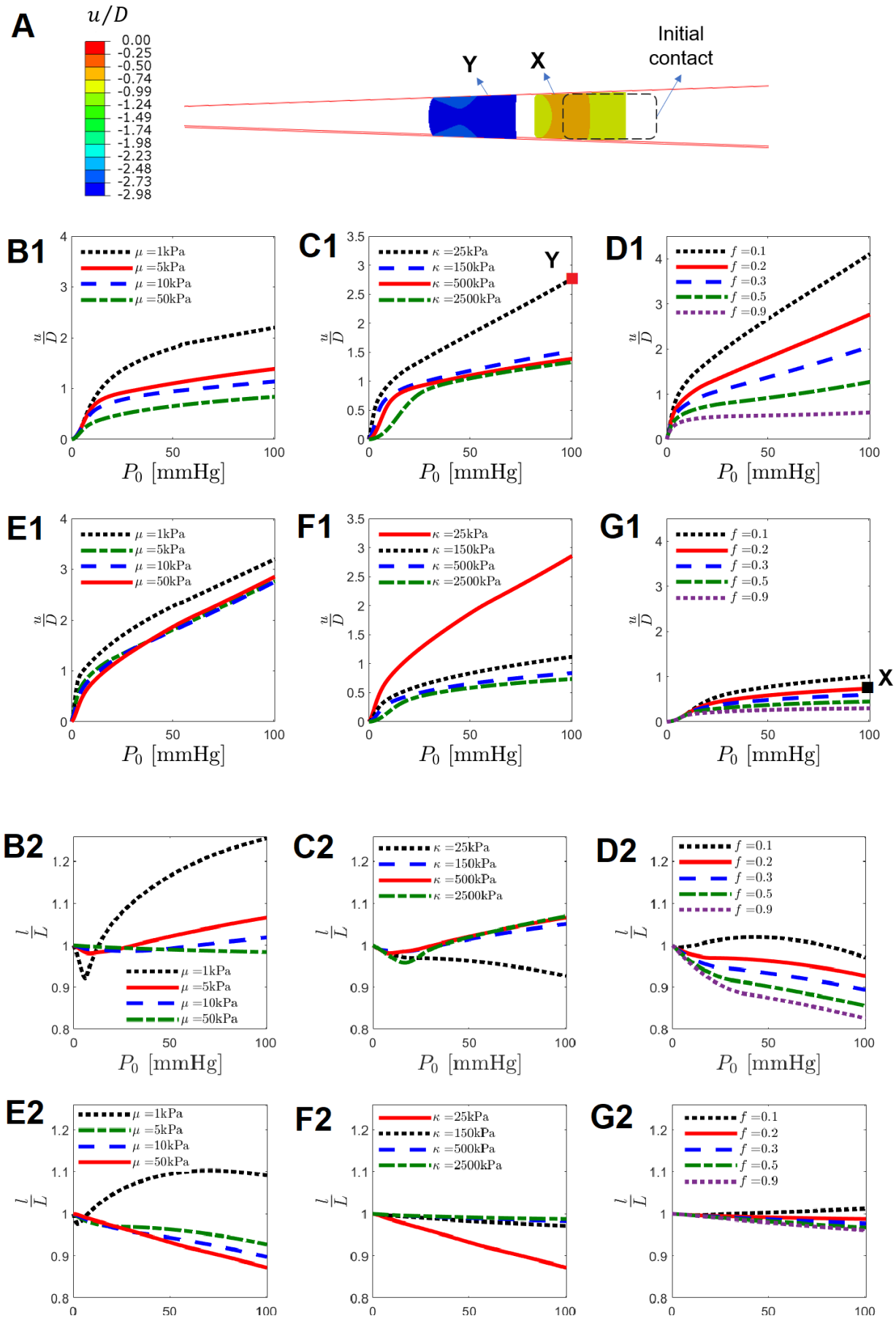
A
u/D
0.00
-0.25
-0.50
-0.74
-0.99
-1.24
-1.49
-1.74
-1.98
-2.23
-2.48
-2.73
-2.98
Y
X
Initial contact
B1
C1
D1
E1
F1
G1
B2
C2
D2
E2
F2
G2
μ =1kPa
μ =5kPa
μ =10kPa
μ =50kPa
κ =25kPa
κ =150kPa
κ =500kPa
κ =2500kPa
f =0.1
f =0.2
f =0.3
f =0.5
f =0.9
P0 [mmHg]
u/D
l/L

Fig.3*: The effects of shear modulus (μ), bulk modulus (κ), and friction coefficient (f) on the occlusion location u in a tapered vessel (B1-G1) and clot length l (B2-G2). The baseline parameters of $L/D = 2, P_0 = 100\, mmHg,\ E_1 = E_2 = 0.0844\, kPa, D_1 = 0.03, D_2 = 0.08, f = 0.2\ and\ \Phi = 2^o$ are used. Also $\kappa = 500\, kPa,\ \kappa = 25\, kPa$ have been used in (B1,B2) and (E1,E2), respectively; $\mu = 5\, kPa, \mu = 50\, kPa$ have been used in (C1,C2) and (F1,F2), respectively; $\mu = 5\, kPa,\ \kappa = 25\, kPa$ have been used in (D1,D2), and $\mu = 50\, kPa,\ \kappa = 2500\, kPa$ have been used for (G1,G2).*

In Fig.4 we further explore the preliminary results by considering the computed values of u, l and $\widehat{\mathrm{AR}}$ at a fixed physiological pressure of $P_0 = 100\ \mathrm{mmHg}$. Fig.4A demonstrates the non-linear dependence of u, l and $\widehat{\mathrm{AR}}$ on shear modulus, while Fig.4B demonstrates the high level of sensitivity of u, l and $\widehat{\mathrm{AR}}$ to bulk modulus below a threshold value of compressibility ($\kappa/P_0 \lesssim 4$), and a contrasting insensitivity to bulk modulus above this threshold value.

Influence of clot aspect ratio

Fig.4C shows the influence of the aspect ratio of the clot ($(AR)_0 = L/D$) on the final equilibrium position, length and final aspect ratio of clot ($\mathrm{AR} = l/d$). As L/D increases (i.e. as a clot of a given diameter becomes longer), the distance travelled (u/D) and the length of clot (l/D) decreases while the aspect ratio (AR) shows a non-monotonic response. This highly non-linear phenomenon is explained in part by the increased friction resistance for longer clots. This model predictions is consistent with the clinical observation that a shorter thrombus is more likely to have a distal location (Dutra et al. 2019; Boodt et al. 2020).

Influence of taper angle of the vessel

In Fig.4D we assess the influence of taper angle of the vessel on u, l and $\widehat{\mathrm{AR}}$. As expected, the value of u is highly sensitive to an increase in taper angle. These analyses can guide the design of tapered-vessel experiments so that the taper angle results in a test system sensitivity range that is capable of differentiating between physiologically relevant clot compositions.

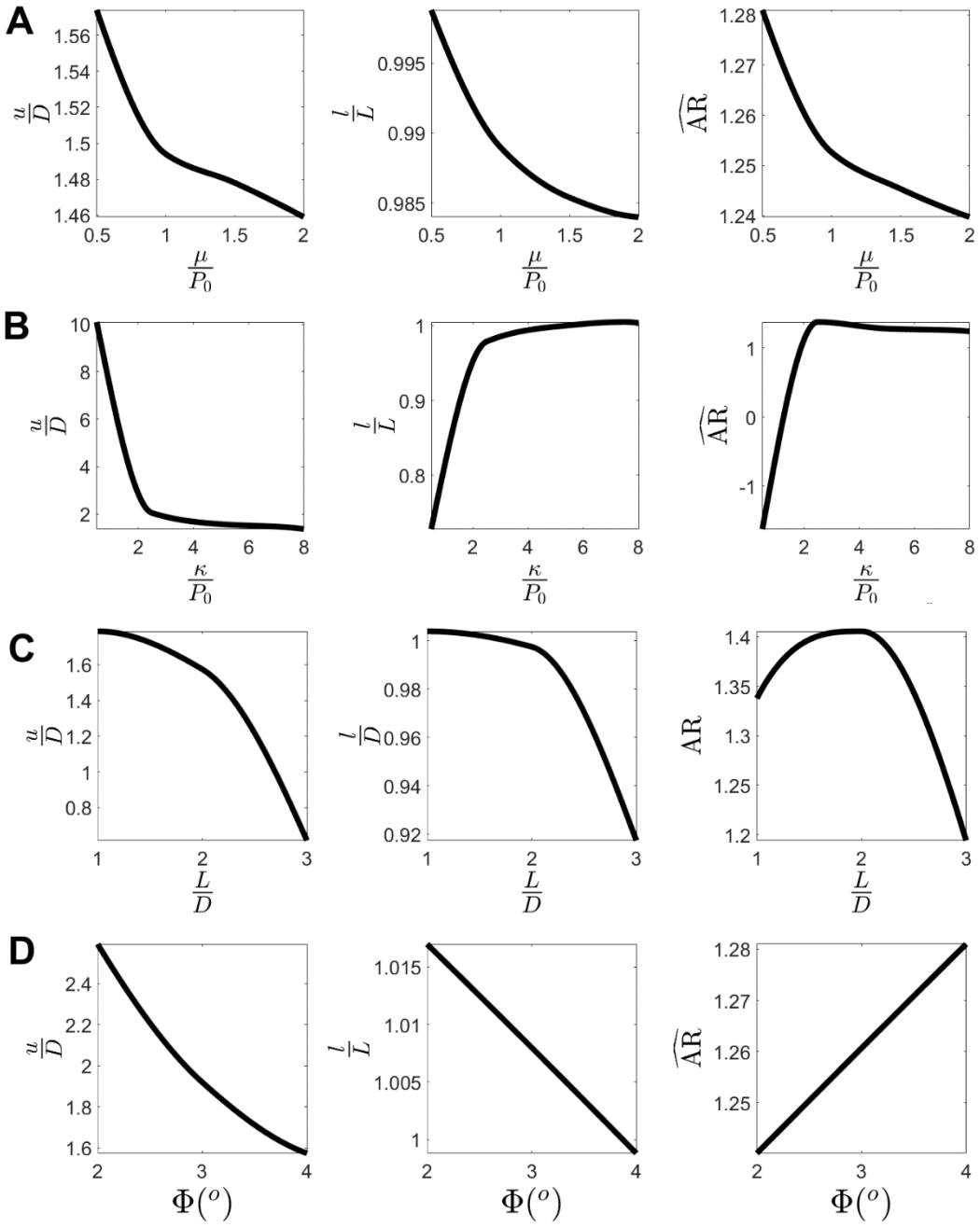

Fig.4*: Influence of (A) the shear modulus μ, (B) the compressibility of clot κ, (C) length to diameter ratio of clot L/D, and (D) tube angle (Φ) on the clot travel through the tapered vessel, length of clot and aspect ratio of clot. Baseline parameters of $L/D = 2, P_0 = 75\ mmHg, \mu = 5\ kPa,\ \kappa = 25\ kPa, E_1 = E_2 = 14.06\ kPa,\ D_1 = 0.03, D_2 = 0.08, f = 0.1, and\ \varphi = 4^o$ are used.*

Interactions between governing parameters

The results presented in Fig.3 and Fig.4 take into account the influence of single system parameters on the occlusion location, assuming a base-line reference value

for all other system parameters. Such preliminary analyses provide a reasonable introduction to the governing mechanism of clot occlusion in a tapered vessel. However, in reality all parameters interact with one another, requiring the computation of response surfaces to provide a more detailed understanding of the system. Such response surfaces for paired-interactions between key system parameters are shown in Fig.5. Fig.5A1 presents a 3D surface that elucidates the $\kappa - \mu$ interactions introduced in Fig.4 above. Fig.5B1 demonstrates that u is sensitive to μ for lower value of friction coefficient, f, while it is insensitive to shear modulus for high values of f. Similar sensitivities are observed in the $\kappa - f$ interactions (Fig.5C1). Fig.5D1 shows the interaction of taper angle, Φ, with f. For very high friction values, u is insensitive to Φ, i.e. once the clot initially contacts the tube, it almost immediately becomes lodged, without significant volumetric or isochoric deformation. However, as f reduces, the sensitivity to Φ increases. Similarly, the sensitivity of u to the values of both κ and μ is increased if the value of Φ is reduced. In summary, a tapered-tube experimental system should implement sufficiently low values of Φ and f so that the measured value of u is sensitive to the clot mechanical properties/composition. Fig.5G1 demonstrates interactions between clot aspect ratio (L/D) and f, while Fig.5H1 demonstrates the interaction between L/D and κ. A low level of sensitivity of u to κ is computed for extremely long clots. This is in part, due to a more dominant role of frictional resistance with increasing clot length. Therefore, low aspect-ratio clots should be used experimentally $L/D < 3$ so that the system is sensitive to the clot material properties. The response surfaces for the influence of the parameters on the length of the clots are also provided in Fig.5A2-H2.

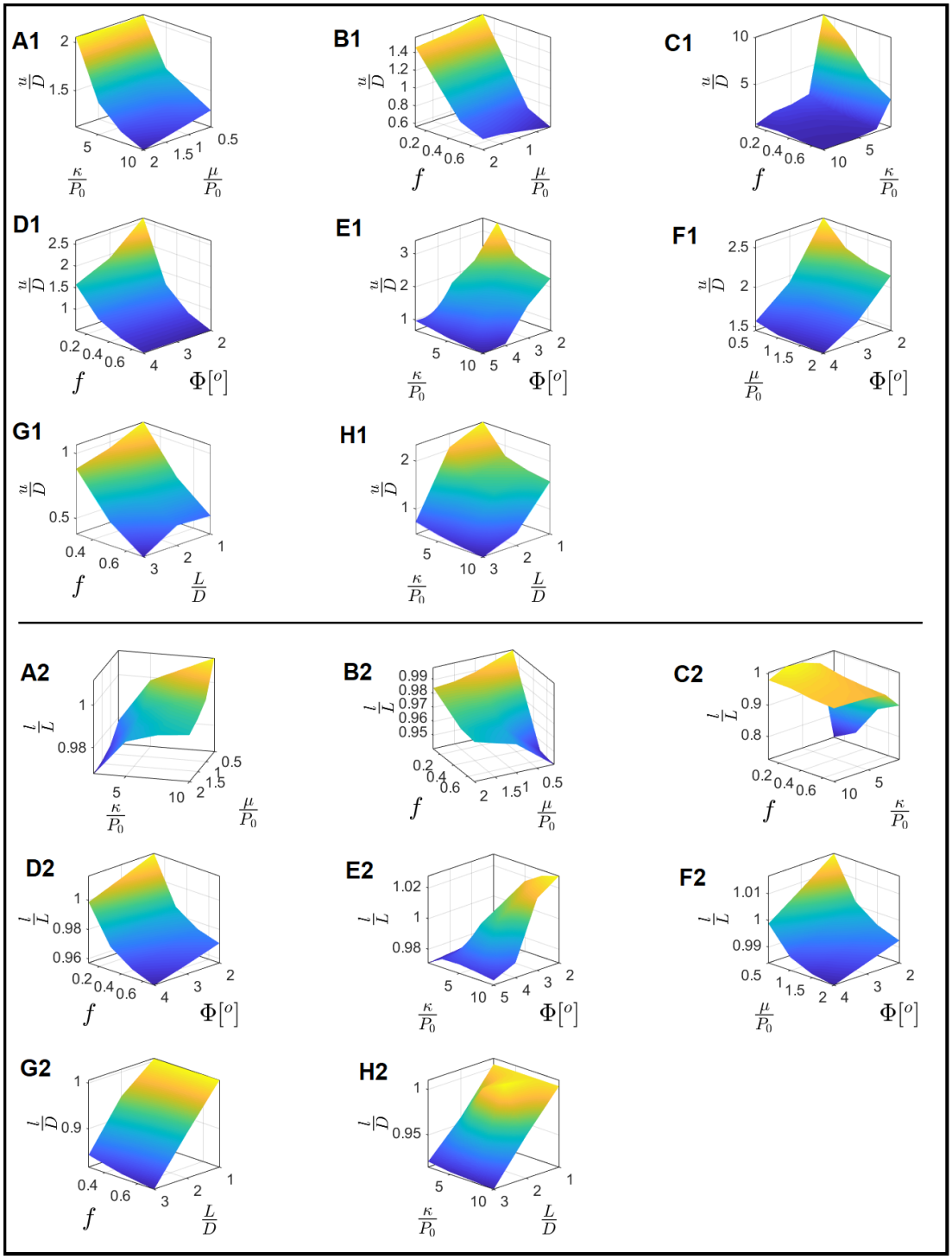

***Fig.5**: Interactions of the model parameters influencing the occlusion location of blood clot and length of clot in a tapered vessel. The baseline parameters are:* $L/D = 2, P_0 = 75\ mmHg, \mu = 5\ kPa,\ \kappa = 25\ kPa, E_1 = E_2 = 14.06\ kPa,\ D_1 = 0.03, D_2 = 0.08, f = 0.1, and\ \Phi = 4^o$.

3.2 Realistic non-linear clot behaviour and vessel deformability

As demonstrated in Fig.1, blood clots exhibit significant volumetric and isochoric strain-stiffening (Johnson et al. 2020). Here, we use the proposed constitutive model in Section 2 to investigate the influence of clot stiffening on the distance travelled (u/D) in a tapered tube. The baseline material parameters are chosen to be the same as those presented in Table 1 for fibrin-rich platelet-contracted clot. Fig.6 demonstrates that for the given parameter sets, strain stiffening of the clot strongly influences the occlusion location. Fig.6B demonstrate that if the stiffening ratio ($\mathrm{E}_2/\mathrm{E}_1$) is increased from 1 to 10, u decreases by 18%. The results of Fig.6D shows even an stronger influence of volumetric stiffening (κ_2/κ_1) on u. Increasing κ_2/κ_1 from 1 to 10 results in a 38% decrease in the value of u. Such sensitivity to κ_2/κ_1 is less pronounced beyond the threshold of $\kappa_2/\kappa_1 > 20$. Fig.6A, C show that u increases with increasing values of the transition strains D_1 and D_{1v}. Increasing the transition strains postpones the start of clot stiffening, allowing the clot to travel further into the tapered tube.

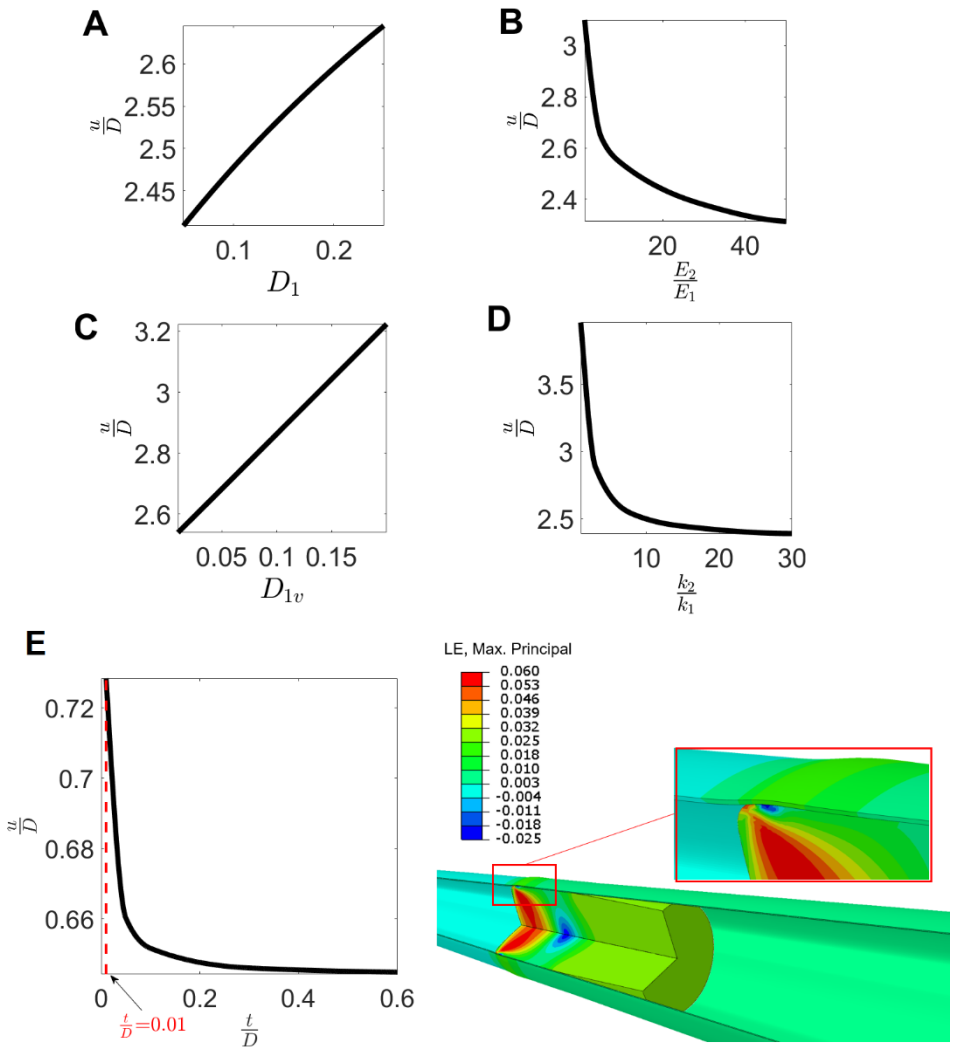

***Fig.6**: Influences of clot strain-stiffening on occlusion location. Effect of (A) the transition strain, D_1; (B) stiffening ratio E_2/E_1; (C) volumetric transition strain D_{1v}, and (D) bulk modulus ratio κ_2/κ_1 are illustrated. The baseline material parameters are taken from Table 1 for fibrin-rich platelet-contracted clot and $L/D = 2$, $P_0 = 75\ mmHg$, $f = 0.2$ and $\Phi = 2^o$ are used. The value of $D_2 - D_1$ and $D_{2v} - D_{1v}$ are kept constant. Influences of tube thickness on the occlusion location for a silicone tapered tube and the deformed shape of the clot in a thin tube (t/D=0.01) is also shown in (E). The inset shows bulge in the tube.*

The validity of modelling the tapered vessel as a rigid body is investigated by incorporating the effect of tube compliance and thickness in the FE simulations. Silicon rubber tubes with a range of thicknesses are considered and the variation of occlusion location with tube thickness is shown in Fig.6E. Results are sensitive to the wall

thickness of a silicone tube only if the tube wall thickness is less than 5% of the clot diameter. As an example, for a clot of 5mm diameter, the tube can reliably be modelled as a rigid material provided that the tube wall thickness is greater than ~250 μm. In Section 3.3 the non-linear compliance of a cerebral artery is taken into account in the simulation of clot occlusion in a patient-specific vessel anatomy.

3.3. Simulation of in-vitro tapered vessel experiment and in-vivo patient specific clot occlusion

In-vitro clot occlusion in a tapered tube:

An in-vitro test rig is developed in which clot analogues are introduced (through a side port) into a tapered silicone vessel, as shown in Fig.7A. The vessel is fabricated with a taper angle of $\Phi = 0.9854^{o}$ (BioMET, GMIT, Galway, Ireland) over a length of 250 mm. The tapered vessel is connected to a pulsatile pump (PD-1100 pulsatile pump, BDC Laboratories), which precisely controls the pulse rate, pressure and temperature of the system. 0.9% saline, which was heated to 37°C was pumped through the model with a pulse rate of 75 BPM. Applied pressures of 90 mmHg and 30 mmHg were applied to the proximal and distal surfaces of the clots, respectively. The clot final occlusion location and deformed shape of the clot are measured. Clot specimens of length 10 mm and diameter 6 mm are fabricated in accordance with previously reported protocols (Johnson et al. 2020). Two platelet-contracted blood clot analogues compositions are considered: made from blood mixtures with 5%H (N=5) and 40%H (N=5). Detailed experimental results for additional clot compositions and characterisation of irregular deformation of proximal clot surfaces are presented in (Johnson 2020).

Simulation of in-vitro tapered vessel experiment:

We have simulated the in-vitro test for a fibrin-rich and a RBC-rich clot using our proposed volumetric and isochoric hyperelastic formulations and compare model predictions to the experimental measurements of Johnson et al. (2020). Using the

material parameters obtained from the compression test (Table 1), we have ran the simulations for five different friction coefficients for the contact between the silicone surface and fibrin-rich and a RBC-rich clot analogues. The results, as demonstrated in Fig.7, reveal that friction coefficients of $f = 0.07$ for 5% H clot and $f = 0.05$ for RBC-rich clot result in a reasonable agreement between computational results and the in-vitro data in terms of the distance that clot travel into the tube (u/D) and the deformation of the clot, characterised by the normalised aspect ratio ($\widehat{\mathrm{AR}}$). This findings are in agreement with the experimental observation of Gunning et al. (2018) that the friction coefficient for a fibrin-rich clot is higher than the friction coefficient for a RBC-rich clot on a PTFE surface.

Despite the fact that the fibrin rich clot has a higher isochoric tangent modulus and friction coefficient, it travels farther into the tapered vessel than the RBC-rich clot. This is due to the higher level of compressibility (volumetric deformability) of the fibrin-rich clot. This suggests that non-linear hyperelastic volumetric behaviour is a key determinant of the occlusion location of a clot. This further highlights the importance of the accurate characterization of and constitutive modelling of the volumetric behaviour of a range of clot compositions. A comparison between the proposed model and Ogden model for prediction of the tapered tube experiment results are also presented in Appendix E.

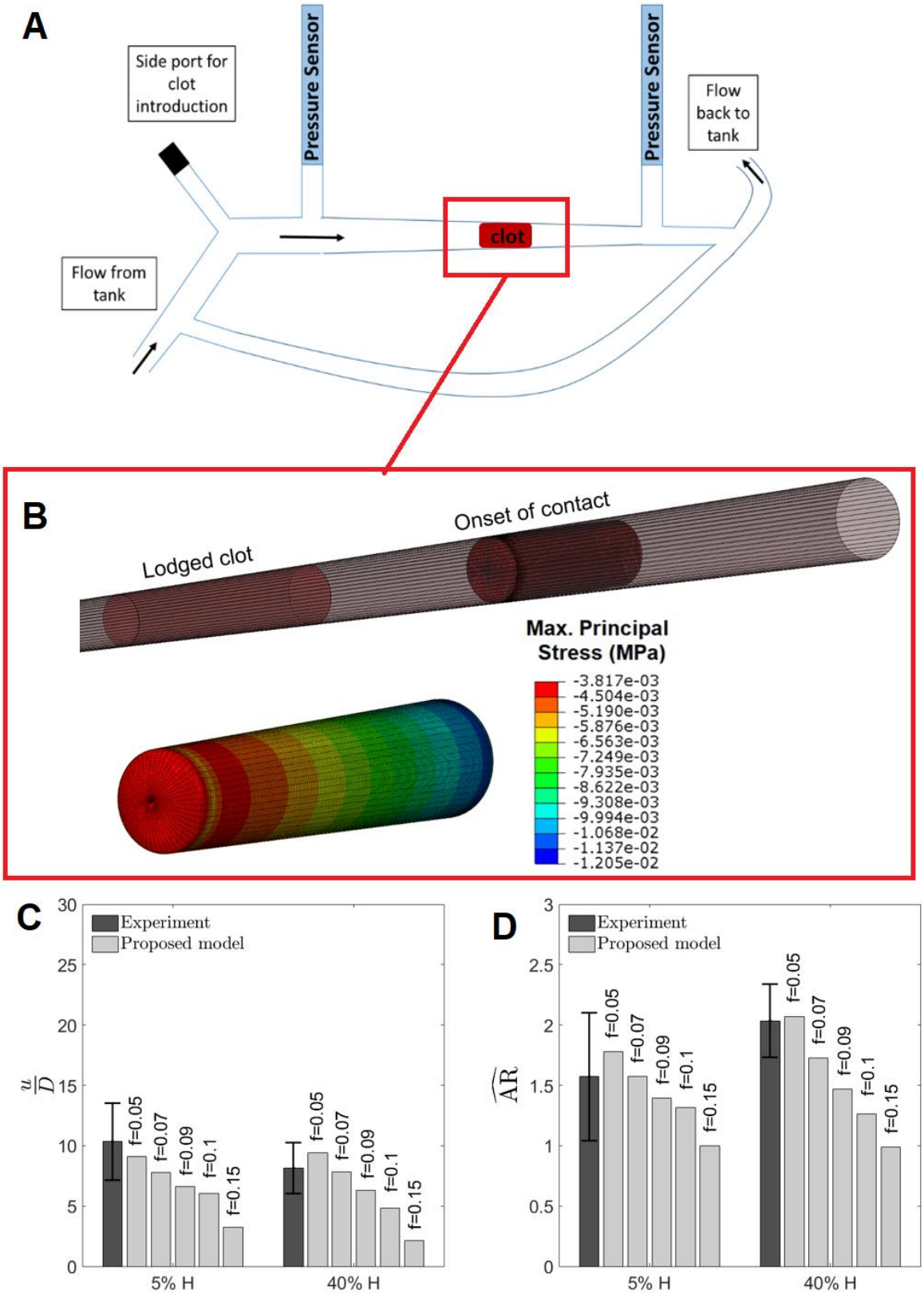

***Fig.7**: Comparison of in-vitro and FE results for occlusion of the platelet-contracted blood clot analogues in a silicon rubber vessel with taper angle of $\Phi = 0.9854^{o}$. (A)*

Schematic of the experimental set-up. (B) FE simulation results for the RBC-rich platelet-contracted clot made from a 40% H blood mixture. (C) The location of clot lodgement (u/D) and (D) aspect ratio of clot ($\widehat{AR}$) for fibrin-rich (5% H) and RBC-rich (40% H) clot. The material parameters from Table 1 have been employed. Experimental results reproduced from Johnson et al. (2020).

Simulation of in-vivo patient specific clot occlusion

Finally, we simulate clot occlusion in a patient-specific cerebral artery. The vessel geometry is reconstructed from clinical CT images using the GIBBON toolbox (Moerman 2018). A portion of the M1 cerebral artery proximal to the occlusion location, based on CT images, has been used in this simulation as shown in Fig. 8A. Both ends of the artery have been fixed and outer surface of the artery is stress free.

A mesh study has been performed to find out the required mesh density for a converged solution. 57398 elements of type C3D4 for clot and 5075 elements of type C3D8 for the artery, with one element through the thickness, have been found enough for convergence of the results. The C3D4 and C3D8 elements have been used for clot and vessel, respectively. The mechanical behaviour of the vessel is based on the experimental test data for cerebral arteries reported by Monson et al. (Monson et al. 2003). Friction coefficient of 0.3 has been used for the contact between artery and clot. A cylindrical-shape RBC-rich platelet-contracted clot, made from a 40% H blood mixture, with length of 11mm and diameter of 3.75 mm is introduced into the vessel (Fig.8B) with a pressure $\mathrm{P}_0 = 75\ \mathrm{mmHg}$ applied to the proximal face of the clot to approximate in-vivo physiological loading.

Fig.8B (top) illustrates the clot at initial point of contact between the clot and the vessel. The final computed deformed clot at the location of occlusion is also shown in Fig.8B (bottom row – three views shown to illustrate vessel tortuosity). The computed distribution of the maximum shear stress, maximum principal stress, and minimum principal stress in the clot at lodged position are shown in Fig.8C, to provide a complete characterisation of the stress state within the clot. This simulation highlights the significant deformation and stress in the clot at its occluded location. Such predicted stress distributions could be included in FE simulations of clinical interventions, such as thrombectomy and aspiration (Luraghi et al. 2021) to provide improved predictions

of the interaction between the clot and the intervention device and may also provide improved prediction of clot fragmentation risk during thrombectomy procedures. For example the maximum principal stress in this simulation is lower than the critical value for clot fracture recently determined by the authors (Fereidoonnezhad et al. 2020a). Finally, the strain and deformation of the arterial wall due to interaction with the clot is shown in Fig.8D. The small values of strain and deformation suggest that modelling the artery geometry as a rigid body is acceptable.

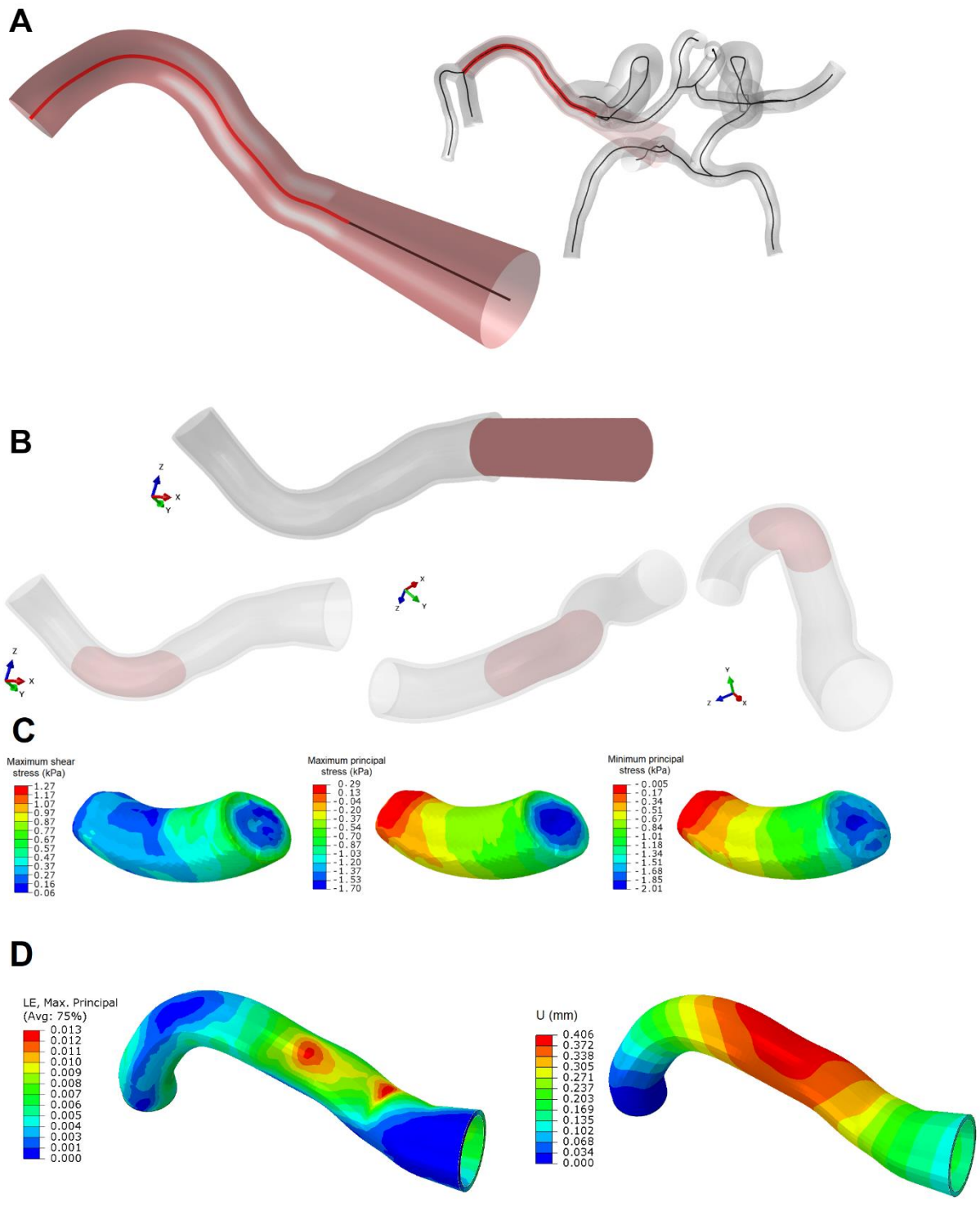

***Fig.8**: FE prediction of the clot occlusion in a patient-specific cerebral artery for a platelet-contracted clot analogue made from 40% H blood mixture. (A) location of the simulated section of the artery in cerebral vasculature (B) Clot at onset of contact and at lodged position, (C) Cauchy stress distribution in the clot at lodged position, and (D) Maximum principal logarithmic strain and displacement of the vessel wall.*

4. Summary and conclusions

Mechanical thrombectomy has become the standard acute ischemic stroke treatment in patients with large vessel occlusion. The success of the thrombectomy procedure can be significantly affected by the mechanical properties of the occluding thrombus. In this study we provide the first characterization of the volumetric behaviour of blood clots. We propose a new hyperelastic model for the volumetric and isochoric deformation of blood clot. We demonstrate that the proposed model provides significant improvements over established hyperelastic models in terms of accurate prediction of nonlinear stress-strain behaviour and non-linear volumetric behaviour of fibrin-rich and RBC-rich blood clots. We perform a rigorous parametric investigation of the factors that govern clot occlusion of a tapered vessel. The motivation for such an analysis are two-fold: (i) the role of clot composition on the in-vivo occlusion location is a key and open clinical question that has significant implications for thrombectomy procedures; (ii) in-vitro benchtop measurement of occlusion location in an engineered tapered tube can potentially be used as a quick and simple methodology to assess the mechanical properties/compositions of excised clots or fabricated clot analogues. Simulations demonstrate that both the isochoric and the volumetric behaviour of blood clots are key determinants of the location of clot lodgement in a tapered vessel, in addition to clot-vessel friction. The proposed volumetric/isochoric clot hyperelastic formulation is shown to provide accurate predictions of in-vitro measurement so of clot occlusion location in a silicone tapered vessel, in addition to accurately predicting the deformed shape of the clot. These findings provides a significant advance in the current understanding of the relationship between clot mechanical behaviour and occlusion location in cerebral vascular network which can help to guide clinical intervention strategies and development of the next-generation thrombectomy devices

The following key points should be noted:

1. The non-linear volumetric and isochoric hyperelastic constitutive law proposed in this study provide accurate predictions of the complex patterns of experimentally measured stress and corresponding volume change for both RBC-rich clots (made form 40% H blood mixture) and fibrin-rich clots (made from 5% H blood mixture). We demonstrate that established hyperelastic models cannot provide comparable levels

of accuracy. Therefore, our model predictions suggests that (i) blood clots transition from a low constant stiffness regime at low strains to a high constant stiffness regime at high strains, rather than exhibiting continuous power-law or exponential strain stiffening; (ii) blood clots exhibit a volumetric strain stiffening, and traditionally implemented single parameter (bulk modulus) linear volumetric constitutive laws (Fereidoonnezhad et al. 2016, 2017; Nolan and McGarry 2016; Rouhani et al. 2019) are not suitable for the simulation of large multiaxial large-deformation of clots. This study provides the first detailed characterisation of the volumetric change for a range of clot analogue compositions.

2. Accurate modelling of volumetric and isochoric behaviour of clots is critical in order to accurately predict clot occlusion location in a tapered vessel. The volumetric and isochoric formulation proposed in the current study is shown to provide a reasonably accurate prediction of in vitro experiments of clot occlusion in a tapered silicone vessel, both in terms of occlusion location and deformed shape of the clot. Accurate predictions are achieved for both fibrin-rich and RBC-rich clots. Our simulation of clot occlusion in patient-specific vessel provides a quantitative distribution of stress throughout the clot when lodged in the vessel. This can be used as an initial condition for in silico thrombectomy simulations (Luraghi et al. 2021) .

The new understanding of volumetric behaviour of clots will be incorporated into ongoing development of in silico models for thrombectomy procedures. Future simulations will consider the multiaxial deformation of the lodged clot due to deployment of stent retrievers (Luraghi et al. 2021). The rupture risk during thrombectomy and aspiration will be simulated using cohesive zone (McGarry and McHugh 2008; McGarry et al. 2014) and extended finite element techniques (Feerick et al. 2013) based on the recent experimental investigation of the influence of clot composition on fracture resistance (Fereidoonnezhad et al. 2020a). The future work should also focus on the relationship between clot composition and occlusion location in patient specific models.

5. Acknowledgements

This work has received funding from the European Union's Horizon 2020 research and innovation programme under grant agreement No 777072.

6. References

Ajjan RA, Standeven KF, Khanbhai M, et al (2009) Effects of aspirin on clot structure and fibrinolysis using a novel in vitro cellular system. Arterioscler Thromb Vasc Biol 29:712–717. https://doi.org/10.1161/ATVBAHA.109.183707

Ashton JH, Vande Geest JP, Simon BR, Haskett DG (2009) Compressive mechanical properties of the intraluminal thrombus in abdominal aortic aneurysms and fibrin-based thrombus mimics. J Biomech 42:197–201. https://doi.org/10.1016/j.jbiomech.2008.10.024

Boodt N, Compagne KCJ, Dutra BG, et al (2020) Stroke Etiology and Thrombus Computed Tomography Characteristics in Patients with Acute Ischemic Stroke: A MR CLEAN Registry Substudy. Stroke 51:1727–1735. https://doi.org/10.1161/STROKEAHA.119.027749

Chueh JY, Wakhloo AK, Hendricks GH, et al (2011) Mechanical characterization of thromboemboli in acute ischemic stroke and laboratory embolus analogs. Am J Neuroradiol 32:1237–1244. https://doi.org/10.3174/ajnr.A2485

Di Martino E, Mantero S, Inzoli F, et al (1998) Biomechanics of abdominal aortic aneurysm in the! presence of endoluminal thrombus: Experimental characterisation and structural static computational analysis. Eur J Vasc Endovasc Surg 15:290–299. https://doi.org/10.1016/S1078-5884(98)80031-2

Duffy S, Farrell M, McArdle K, et al (2017) Novel methodology to replicate clot analogs with diverse composition in acute ischemic stroke. J Neurointerv Surg 9:486–491. https://doi.org/10.1136/neurintsurg-2016-012308

Dutra BG, Tolhuisen ML, Alves HCBR, et al (2019) Thrombus Imaging Characteristics and Outcomes in Acute Ischemic Stroke Patients Undergoing Endovascular Treatment. Stroke 50:2057–2064. https://doi.org/10.1161/STROKEAHA.118.024247

Feerick EM, Liu XC, McGarry P (2013) Anisotropic mode-dependent damage of cortical bone using the extended finite element method (XFEM). J Mech Behav Biomed Mater 20:77–89. https://doi.org/10.1016/j.jmbbm.2012.12.004

Fereidoonnezhad B, Dwivedi A, Johnson S, et al (2020a) Blood clot fracture properties are dependent on red blood cell and fibrin content. Acta Biomater (under review): https://doi.org/10.1101/2020.10.05.326165.

Fereidoonnezhad B, Naghdabadi R, Holzapfel GA (2016) Stress softening and permanent deformation in human aortas: Continuum and computational modeling with application to arterial clamping. J Mech Behav Biomed Mater 61:. https://doi.org/10.1016/j.jmbbm.2016.03.026

Fereidoonnezhad B, Naghdabadi R, Sohrabpour S, Holzapfel GA (2017) A Mechanobiological model for damage-induced growth in arterial tissue with application to in-stent restenosis. J Mech Phys Solids 101:. https://doi.org/10.1016/j.jmps.2017.01.016

Fereidoonnezhad B, O'Connor C, McGarry P (2020b) A new anisotropic soft tissue model for elimination of unphysical auxetic behaviour. J Biomech. https://doi.org/10.31224/OSF.IO/G6DSE

Gabbay JS, Zuk PA, Tahernia A, et al (2006) *In Vitro* Microdistraction of Preosteoblasts: Distraction Promotes Proliferation and Oscillation Promotes Differentiation. Tissue Eng 12:3055–3065. https://doi.org/10.1089/ten.2006.12.3055

Gasser TC, Görgülü G, Folkesson M, Swedenborg J (2008) Failure properties of intraluminal thrombus in abdominal aortic aneurysm under static and pulsating mechanical loads. J Vasc Surg 48:179–188. https://doi.org/10.1016/j.jvs.2008.01.036

Gunning GM, McArdle K, Mirza M, et al (2018) Clot friction variation with fibrin content; implications for resistance to thrombectomy. J Neurointerv Surg 10:34–38. https://doi.org/10.1136/neurintsurg-2016-012721

Johnson S (2020) Thrombus analogue material: Mechanical characterisation and use in in-vitro modelling of acute ischemic stroke treatment, (Doctoral dissertation, NUI Galway).

Johnson S, Chueh J, Gounis MJ, et al (2019) Mechanical behavior of in vitro blood

clots and the implications for acute ischemic stroke treatment. J Neurointerv Surg 1–6. https://doi.org/10.1136/neurintsurg-2019-015489

Johnson S, Ray McCarthy, Peter McHugh, et al (2020) Investigating the Mechanical Behaviour of Clot Analogues through Experimental and Computational Analysis. Ann Biomed Eng 1–12. https://doi.org/10.1007/s10439-020-02570-5

Kim J, Srinivasan MA (2005) Characterization of viscoelastic soft tissue properties from in vivo animal experiments and inverse FE parameter estimation. In: Lecture Notes in Computer Science (including subseries Lecture Notes in Artificial Intelligence and Lecture Notes in Bioinformatics). Springer, Berlin, Heidelberg, pp 599–606

Krasokha N, Theisen W, Reese S, et al (2010) Mechanical properties of blood clots - a new test method. Mechanische Eigenschaften von Thromben - Neue Untersuchungsmethoden. Materwiss Werksttech 41:1019–1024. https://doi.org/10.1002/mawe.201000703

Liebeskind DS (2005) Collaterals in acute stroke: Beyond the clot. Neuroimaging Clin N Am 15:553–573. https://doi.org/10.1016/j.nic.2005.08.012

Luraghi G, Rodriguez Matas JF, Dubini G, et al (2021) Applicability assessment of a stent-retriever thrombectomy finite-element model. Interface Focus 11:20190123. https://doi.org/10.1098/rsfs.2019.0123

Malone F, McCarthy E, Delassus P, et al (2018) The Mechanical Characterisation of Bovine Embolus Analogues Under Various Loading Conditions. Cardiovasc Eng Technol 9:489–502. https://doi.org/10.1007/s13239-018-0352-3

McEvoy E, Holzapfel GA, McGarry P (2018) Compressibility and Anisotropy of the Ventricular Myocardium: Experimental Analysis and Microstructural Modeling. J Biomech Eng 140:081004. https://doi.org/10.1115/1.4039947

McGarry JP, McHugh PE (2008) Modelling of in vitro chondrocyte detachment. J Mech Phys Solids 56:1554–1565. https://doi.org/10.1016/j.jmps.2007.08.001

McGarry JP, Ó Máirtín É, Parry G, Beltz GE (2014) Potential-based and non-potential-

based cohesive zone formulations under mixed-mode separation and over-closure. Part I: Theoretical analysis. J Mech Phys Solids 63:336–362. https://doi.org/10.1016/j.jmps.2013.08.020

Moerman KM (2018) GIBBON: The Geometry and Image-Based Bioengineering add-On Software • Review • Repository • Archive. https://doi.org/10.21105/joss.00506

Moerman KM, Fereidoonnezhad B, McGarry JP (2020) Novel hyperelastic models for large volumetric deformations. Int J Solids Struct 193–194:474–491. https://doi.org/10.1016/j.ijsolstr.2020.01.019

Monson KL, Goldsmith W, Barbaro NM, Manley GT (2003) Axial mechanical properties of fresh human cerebral blood vessels. J Biomech Eng 125:288–294. https://doi.org/10.1115/1.1554412

Nolan DR, McGarry JP (2016) On the Compressibility of Arterial Tissue. Ann Biomed Eng 44:993–1007. https://doi.org/10.1007/s10439-015-1417-1

Pires PW, Dams Ramos CM, Matin N, Dorrance AM (2013) The effects of hypertension on the cerebral circulation. Am. J. Physiol. - Hear. Circ. Physiol. 304:H1598

Rouhani F, Fereidoonnezhad B, Zakerzadeh MR, Baghani M (2019) A computational study on vascular damage caused by shape memory alloy self-expandable and balloon-expandable stents in a stenosed artery. J Intell Mater Syst Struct 30:3113–3123. https://doi.org/10.1177/1045389X19880021

Saldívar E, Orje JN, Ruggeri ZM (2002) Tensile destruction test as an estimation of partial proteolysis in fibrin clots. Am J Hematol 71:119–127. https://doi.org/10.1002/ajh.10199

Slaboch CL, Alber MS, Rosen ED, Ovaert TC (2012) Mechano-rheological properties of the murine thrombus determined via nanoindentation and finite element modeling. J Mech Behav Biomed Mater 10:75–86. https://doi.org/10.1016/j.jmbbm.2012.02.012

van Dam, Evelyne A. Dams, Susanne D. Peters, Gerrit W.M. Rutten, Marcel C.M.;

Schurink, Geert Willem H. Buth, Jaap van de Vosse FN (2006) Determination of linear viscoelastic behavior of abdominal aortic aneurysm thrombus - IOS Press. https://content.iospress.com/articles/biorheology/bir439. Accessed 18 Jun 2020

Vande Geest JP, Sacks MS, Vorp DA (2006) A planar biaxial constitutive relation for the luminal layer of intra-luminal thrombus in abdominal aortic aneurysms. J Biomech 39:2347–2354. https://doi.org/10.1016/j.jbiomech.2006.05.011

Weafer FM, Duffy S, Machado I, et al (2019) Characterization of strut indentation during mechanical thrombectomy in acute ischemic stroke clot analogs. J Neurointerv Surg 11:891–897. https://doi.org/10.1136/neurintsurg-2018-014601

Zhao S, Gu L, Froemming SR (2011) Assessment of shape memory alloy stent deployment in a stenosed artery. Biomed Eng Lett 1:226–231. https://doi.org/10.1007/s13534-011-0036-5

(2017) Abaqus 2017. Analysis User's Guide, Dassault Systèmes Simulia Corp.

Appendix A: Sensitivity analysis of the proposed model

Sensitivity of nominal stress and volumetric strain to the material model is shown in Fig.A1. As shown in Fig.A1 (E-H), the stress-strain response is not sensitive to the volumetric parameters ($D_{1v}, D_{2v}, \kappa_1, \kappa_2$), however these parameters can control the volumetric strain (ϵ_v). On the other hand, as shown in Fig.A1 (C, D) the stiffness coefficients E_1, E_2, affect both stress-strain and the volumetric behaviour.

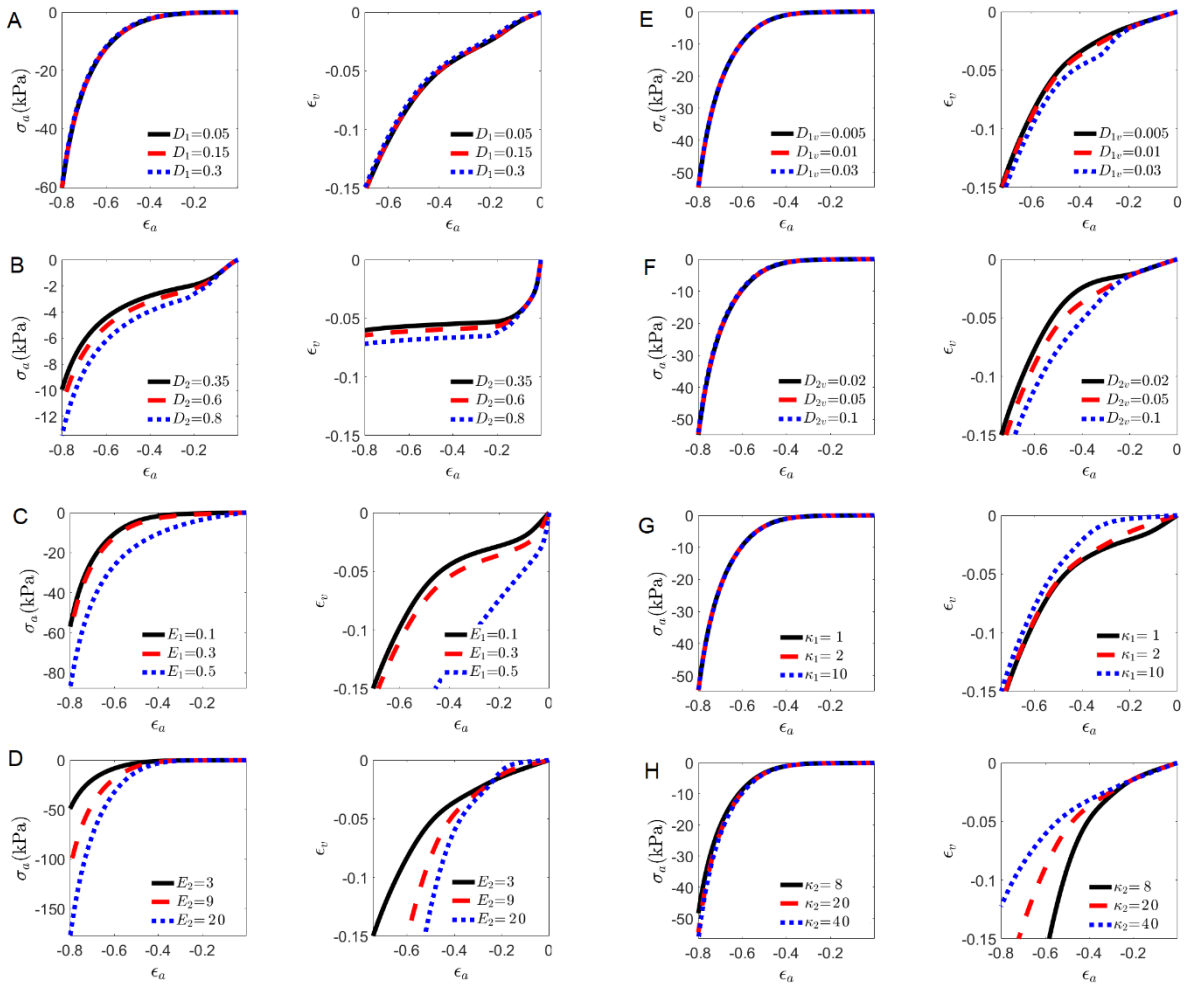

Fig.A1*: Sensitivity analysis of the proposed model in terms of the isochoric and volumetric parameters. Baseline parameters of* $D_1 = 0.15, D_2 = 0.6, E_1 = 0.3\ kPa, E_2 = 9.0\ kPa, D_{1v} = 0.01, D_{2v} = 0.05, \kappa_1 = 2\ kPa, \kappa_2 = 20\ kPa$*, have been used.*

Appendix B: Constitutive models formulations and parameters

The model formulations and best-fit parameters for the hyperelastic models used in Section 2 are presented here. The strain energy density function for Ogden model is given as

$$\psi = \sum_{i=1}^{N} \frac{2\mu_i}{\alpha_i^2}\left(\bar{\lambda}_1^{\alpha_i} + \bar{\lambda}_2^{\alpha_i} + \bar{\lambda}_3^{\alpha_i} - 3\right) + \sum_{i=1}^{N} \frac{1}{D_i}(\mathrm{J}-1)^{2i} \tag{A1}$$

where, μ_i, α_i, and D_i are material parameters. The Yeoh strain energy density function is given as

$$\begin{aligned}\psi = {} & C_{10}(\bar{I}_1 - 3) + C_{20}(\bar{I}_1 - 3)^2 + C_{30}(\bar{I}_1 - 3)^3 \\ & + \frac{1}{D_1}(\mathrm{J}-1)^2 + \frac{1}{D_2}(\mathrm{J}-1)^4 + \frac{1}{D_3}(\mathrm{J}-1)^6,\end{aligned} \tag{A2}$$

where C_{i0} and D_i are material parameters; $\bar{I}_1$ is the first deviatoric strain invariant defined as

$$\bar{I}_1 = \bar{\lambda}_1^2 + \bar{\lambda}_2^2 + \bar{\lambda}_3^2 \tag{A3}$$

The hyperfoam strain energy density function is given as

$$\psi = \sum_{i=1}^{N} \frac{2\mu_i}{\alpha_i^2}\left[\bar{\lambda}_1^{\alpha_i} + \bar{\lambda}_2^{\alpha_i} + \bar{\lambda}_3^{\alpha_i} - 3 + \frac{1}{\beta_i}\left(\mathrm{J}^{-\alpha_i\beta_i} - 1\right)\right] \tag{A4}$$

The best-fit parameters of the aforementioned models for the RBC-rich platelet-contracted clot analogous, corresponding to Fig.1(G, H) is presented in Table B1.

Table B1*: Material parameters of the Ogden, Yeoh, and hyperfoam models for RBC-rich platelet-contracted clot analogues (made from a 40% H blood mixture).*

Ogden model (N=3)								
$\boldsymbol{\mu_1\,(kPa)}$	$\boldsymbol{\alpha_1}$	$\boldsymbol{\mu_2\,(kPa)}$	$\boldsymbol{\alpha_2}$	$\boldsymbol{\mu_3\,(kPa)}$	$\boldsymbol{\alpha_3}$	$\boldsymbol{D_1\,(1/kPa)}$	$\boldsymbol{D_2\,(1/kPa)}$	$\boldsymbol{D_3\,(1/kPa)}$
0.00812	6.41	0.00248	-5.40	0.00009	5.16	207.43	193.37	473.03
Yeoh model								
$\boldsymbol{C_{10}}$	$\boldsymbol{C_{20}}$	$\boldsymbol{C_{30}}$	$\boldsymbol{D_1}$	$\boldsymbol{D_2}$	$\boldsymbol{D_3}$			
0.012	0.025	1e-3	0.1266	0.1266	0.1266			
Hyperfoam model (N=3)								
$\boldsymbol{\mu_1\,(kPa)}$	$\boldsymbol{\alpha_1}$	$\boldsymbol{\mu_2\,(kPa)}$	$\boldsymbol{\alpha_2}$	$\boldsymbol{\mu_3\,(kPa)}$	$\boldsymbol{\alpha_3}$	$\boldsymbol{\beta_1}$	$\boldsymbol{\beta_2}$	$\boldsymbol{\beta_3}$
0.03820	5.91	0.03348	-2.90	0.02598	5.91	0.4845	0.4904	0.4845

Appendix C: Influence of the clot viscoelasticity

Recent experimental data show that thrombus material exhibits rate-dependent visco-hyperelastic behaviour (Johnson et al. 2020). To investigate the influence of viscoelastic behaviour of thrombus material on the occlusion location, we have used the Kelvin-Voigt model where the behaviour of the viscos element is implemented through the specification of a non-dimensional stress-relaxation curve, parameterised through a Prony series and the proposed hyperelastic model has been used for the elastic element. The dimensionless shear-relaxation modulus $\bar{g}(t)$ and the dimensionless volumetric-relaxation modulus $\bar{\kappa}(t)$ in Prony series is given as

$$\bar{g}(t) = 1 - \sum_{i=1}^{n} g_i\left(1 - \exp(-t/\tau_i)\right) \quad \text{(B1)}$$

$$\bar{\kappa}(t) = 1 - \sum_{i=1}^{n} \kappa_i\left(1 - \exp(-t/\tau_i)\right) \quad \text{(B2)}$$

where n is the number of the terms in the Prony series, τ_i are the relaxation time constants for each term of the series, while the parameters g_i and κ_i sets the ratio of long-term to instantaneous effective shear and bulk modulus, respectively. A two term Prony series is implemented with $g_1 = 0.15, g_2 = 0.28, \tau_1 = 60\ \text{sec}, \tau_2 = 500\ \text{sec}$ based on a previous study from our group.

In Fig.C1 two regimes of applied pressure are simulated: a single-step pressure increase, and a multi-step pressure increase. In both cases the clot eventually reaches the same final position. However, even for the case of the single-step pressure increase the clot does not reach its final position until ~400 s after the pressure application. This suggest that tapered tube experimental measurements should be executed over several minutes following pressure application. On the other end of the spectrum, this result suggests that in vivo a clot will reach its final occluded position in the vasculature at a relatively fast time-scale of several minutes, compared to the typical elapsed time (hours) prior to clinical intervention (e.g. thrombectomy).

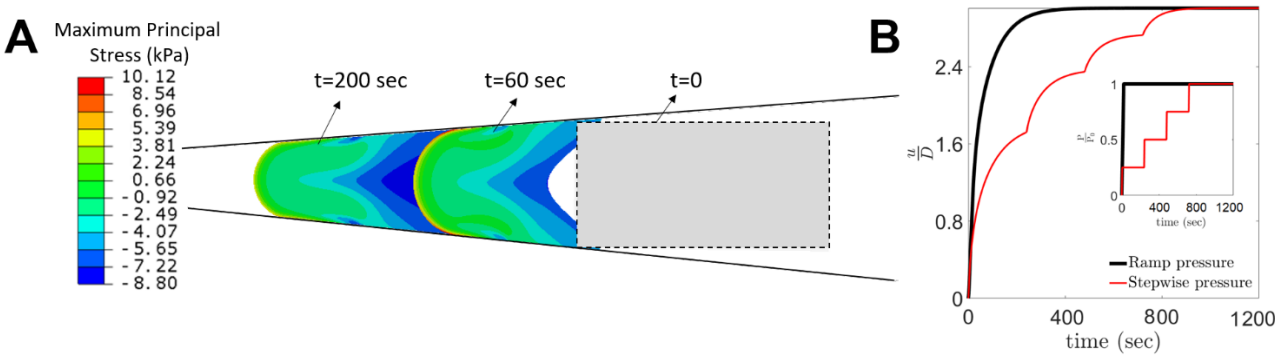

***Fig.C1**: Influences of clot viscoelasticity on the occlusion location, u/D, in a tapered vessel. Variation of the occlusion location with time for two loading profiles (A) are shown in (B). The following parameters have been used , $P_0 = 75\ mmHg$, $L/D = 2$, $\Phi = 5^o$, $f = 0.2$, with the material parameters of the fibrin-rich clot from Table 1 .*

Appendix D: Convergence study

A typical mesh study as a proof of convergence of the results in terms of number of elements is shown in Fig.D1. The dimensions of clot and geometry of the tube is the same of the in vitro test (Section 3.3). The material parameters for the RBC-rich clot from Table 1 and friction coefficient of 0.09 have been used.

Based on the results in Fig.D1, the element size of 0.09 mm (33000 elements for this case) has been considered as the final mesh size and all simulations of the tapered tube in this paper have been performed with this element size.

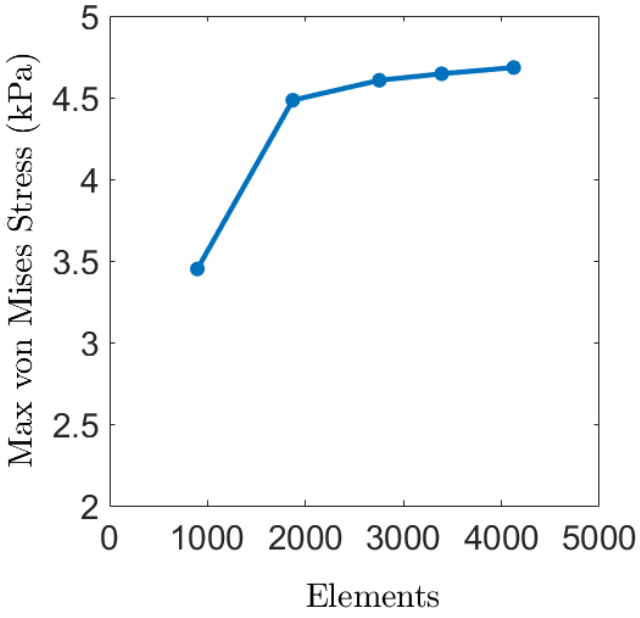

Fig.D1: Variation of the maximum von-Mises stress in clot with the number of elements.

Appendix E: Comparison between the proposed model and Ogden model in taper tube test

We have simulated the tapered tube test by using the Ogden model, with the optimised material parameters in Table A1, for 5 different friction coefficients and the results are compared with the proposed model (Fig. E1). Ogden model was shown to replicate the stress-strain behaviour of clot with acceptable accuracy (Fig. 1G). However, the volumetric behaviour is a key determinant in tapered tube experiment and the proposed volumetric model improve the prediction of the results of tapered tube experiment, as demonstrated in Fig.E1.

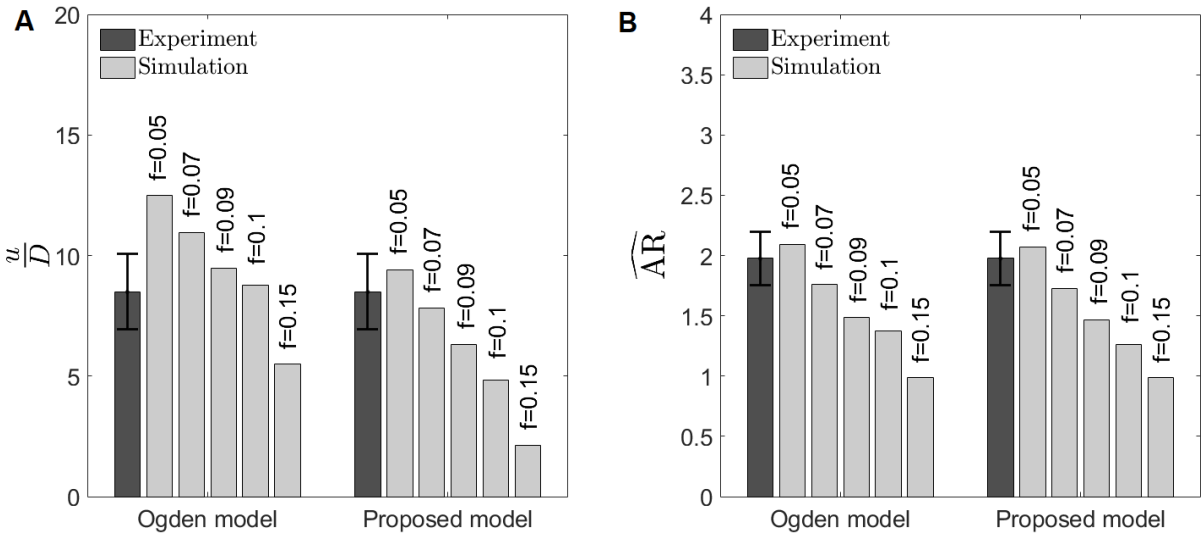

Fig.E1*: Comparison of Ogden and proposed model with the in-vitro experiments of occlusion of the platelet-contracted RBC-rich blood clot analogues (made from a 40% H clot mixture) in a silicon rubber vessel with taper angle of* $\Phi = 0.9854^{o}$*. (A) The location of clot lodgement* (u/D) *and (B) aspect ratio of clot* $(\widehat{AR})$*. The material parameters from Table 1 have been employed. Experimental results reproduced from Johnson et al. (2020).*